

The dynamics of starvation and recovery

2 Justin D. Yeakel * †‡, Christopher P. Kempes †, and Sidney Redner †§

3 *School of Natural Science, University of California Merced, Merced, CA, †The Santa Fe Institute, Santa Fe, NM, §Department of Physics, Boston University, Boston
4 MA, and ‡To whom correspondence should be addressed: jdyeakel@gmail.com

5 Submitted to Proceedings of the National Academy of Sciences of the United States of America

6 We introduce a minimal foraging model that incorporates two
7 classes of foragers: nutritionally replete foragers that can pro-
8 create, and undernourished and non-breeding foragers that
9 are susceptible to mortality. As a function of the transition rates
10 between these replete and undernourished states that are deter-
11 mined by the presence or absence of resources, as well as the
12 replenishment rate of the underlying resource, the forager pop-
13ulations can either undergo cyclic dynamics or reach a steady
14 state. By applying basic allometric considerations, we obtain
15 strong constraints on these transition rates and thereby find that
16 the population dynamics that is subject to these constraints is
17 typically driven to a steady state. As a further consequence of
18 this viewpoint, we find that allometrically constrained rates fall
19 within a ‘refuge’ in parameter space, where the probability of ex-
20 tinction of the consumer population is minimized. Thus our model
21 provides a mechanism that may both drive and constrain natural
22 animal populations. We also find that our model provides a nat-
23ural framework to determine a natural size for animal populations
24 by examining the relative stability of a otherwise homoegeneous
25 population to a mutant population of a different size. For body
26 masses $\lesssim 10^6$ g, a more massive invader dominates over the res-
27 ident population, and vice versa for body mass $\gtrsim 10^6$ g, thus pro-
28 viding a simple principled mechanism for Cope’s rule.

29 foraging | starvation | reproduction

30 Introduction

31 The behavioral ecology of most, if not all, organisms is influ-
32 enced by the energetic state of individuals, which directly influ-
33 ences how they invest reserves in uncertain environments. Such
34 behaviors are generally manifested as trade-offs between invest-
35 ing in somatic maintenance and growth, or allocating energy
36 towards reproduction [1, 2, 3]. The timing of these behaviors
37 responds to selective pressure, as the choice of the investment
38 impacts future fitness [4]. The influence of resource limitation
39 on an organism’s ability to maintain its nutritional stores may
40 lead to repeated delays or shifts in reproduction over the course
41 of an organism’s life.

42 The life history of most species is typically comprised of
43 (a) somatic growth and maintenance, and (b) reproduction.
44 The balance between these two activities is often conditioned
45 on resource availability [5]. For example, reindeer invest less
46 in calves born after harsh winters (when the mother’s ener-
47 getic state is depleted) than in calves born after moderate win-
48 ters [6]. Many bird species invest differently in broods during
49 periods of resource scarcity compared to normal periods [7, 8],
50 sometimes delaying or even foregoing reproduction for a breed-
51 ing season [1, 9, 10]. Even freshwater and marine zooplank-
52 ton have been observed to avoid reproduction under nutritional
53 stress [11], and those that do reproduce have lower survival
54 rates [2]. Organisms may also separate maintenance and growth
55 from reproduction over space and time: many salmonids, birds,
56 and some mammals return to migratory breeding grounds to
57 reproduce after one or multiple seasons in resource-rich environ-
58 ments where they accumulate nutritional reserves [12, 13, 14].

59 Physiological mechanisms also play an important role in
60 regulating reproductive expenditures during periods of resource
61 limitation. The data collected thus far has shown that diverse
62 mammals (47 species in 10 families) exhibit delayed implanta-
63 tion, whereby females postpone fetal development (blastocyst

64 implantation) until times where nutritional reserves can be ac-
65 cumulated [15, 16]. Many other many species (including hu-
66 mans) suffer irregular menstrual cycling and higher spontaneous
67 abortion rates during periods of nutritional stress [17, 18]. In
68 the extreme case of unicellular organisms, nutrition is unavoid-
69 ably linked to reproduction because the nutritional state of the
70 cell regulates all aspects of the cell cycle [19]. The existence of so
71 many independently evolved mechanisms across such a diverse
72 suite of organisms highlights the importance and universality
73 of the fundamental tradeoff between somatic and reproductive
74 investment. However the dynamic implications of these con-
75 straints are unknown.

76 Though straightforward conceptually, incorporating the en-
77 ergetic dynamics of individuals [20] into a population-level
78 framework [20, 21] presents numerous mathematical obsta-
79 cles [22]. An alternative approach involves modeling the
80 macroscale relations that guide somatic versus reproductive
81 investment in a consumer-resource system. For example,
82 macroscale Lotka-Volterra models assume that the growth rate
83 of the consumer population depends on resource density, thus
84 implicitly incorporating the requirement of resource availability
85 for reproduction [23].

86 In this work, we adopt an alternative approach in which
87 resource limitation and the subsequent effect of starvation is
88 accounted for explicitly. Namely, only individuals with suffi-
89 cient energetic reserves can reproduce. Such a constraint leads
90 to reproductive time lags due to some members of the pop-
91 ulation going hungry and then recovering. Additionally, we
92 incorporate the idea that reproduction is strongly constrained
93 allometrically [3], and is not generally linearly related to re-
94 source density. As we shall show, these constraints influence
95 the ensuing population dynamics in dramatic ways.

96 Nutritional-state-structured model (NSM)

97 We begin by defining a minimal Nutritional-State-structured
98 population Model (NSM), where the consumer population is
99 divided into two energetic states: (a) an energetically replete
100 state F , where the consumer reproduces at a constant
101 rate λ and has no mortality risk, and (b) an energetically defi-
102 cient (hungry) state H , where the consumer does not reproduce
103 but dies at rate μ . The underlying resource R evolves by logistic
104 growth with an intrinsic growth rate α and a carrying capacity
105 equal to one. Consumers transition from the full state F to
106 the hungry state H at a rate σ —the starvation rate—and also
107 in proportion to the absence of resources ($1 - R$). Conversely,
108 in proportion to the absence of resources ($1 - R$). Conversely,

Reserved for Publication Footnotes

109 consumers recover from state H to state F at rate ρ and in pro-
 110 portion to R . Resources are also eaten by the consumers—at
 111 rate ρ by hungry consumers and at rate $\beta < \rho$ by full consumers.
 112 This inequality accounts for hungry consumers requiring more
 113 resources to rebuild body weight.

114 In the mean-field approximation, in which the consumers
 115 and resources are perfectly mixed, their densities evolve accord-
 116 ing to the rate equations

$$\begin{aligned}\dot{F} &= \lambda F + \rho RH - \sigma(1-R)F, \\ \dot{H} &= \sigma(1-R)F - \rho RH - \mu H, \\ \dot{R} &= \alpha R(1-R) - R(\rho H + \beta F).\end{aligned}$$

117 Notice that the total consumer density $F + H$ evolves accord-
 118 ing to $\dot{F} + \dot{H} = \lambda F - \mu H$. This resembles the equation of
 119 motion for the predator density in the classic Lotka-Volterra
 120 model, except that the resource density does not appear in the
 121 growth term. As discussed above, the attributes of reproduc-
 122 tion and mortality have been explicitly apportioned to the full
 123 and hungry consumers, respectively, so that the growth in the
 124 total density is decoupled from the resource density.

125 Equation [1] has three fixed points: two trivial fixed points
 126 at $(F^*, H^*, R^*) = (0, 0, 0)$ and $(0, 0, 1)$, and one non-trivial,
 127 internal fixed point at

$$\begin{aligned}F^* &= \frac{\alpha\lambda\mu(\mu+\rho)}{(\lambda\rho+\mu\sigma)(\lambda\rho+\mu\beta)}, \\ H^* &= \frac{\alpha\lambda^2(\mu+\rho)}{(\lambda\rho+\mu\sigma)(\lambda\rho+\mu\beta)}, \\ R^* &= \frac{\mu(\sigma-\lambda)}{\lambda\rho+\mu\sigma}.\end{aligned}$$

128 The stability of this fixed point is determined by the Jaco-
 129 bian Matrix \mathbf{J} , where each matrix element J_{ij} equals $\partial\dot{X}_i/\partial X_j$
 130 when evaluated at the internal fixed point, and \mathbf{X} is the vec-
 131 tor (F, H, R) . The parameters in Eq. [1] are such that the
 132 real part of the largest eigenvalue of \mathbf{J} is negative, so that the
 133 system is stable with respect to small perturbations from the
 134 fixed point. Because this fixed point is unique, it is the global
 135 attractor for all population trajectories for any initial condition
 136 where the resource and consumer densities are both non zero.

137 From Eq. [2], an obvious constraint on the NSM is that
 138 the reproduction rate λ must be less than the starvation rate
 139 σ , so that R^* is positive. In fact, when the resource density
 140 $R = 0$, the rate equation for F gives exponential growth of
 141 F for $\lambda > \sigma$. The condition $\sigma = \lambda$ represents a transcritical
 142 (TC) bifurcation that demarcates the physical and unphysical
 143 regimes [give Ref]. The biological implication of the constraint
 144 $\lambda < \sigma$ has a simple interpretation—the rate at which a macro-
 145 scopic organism loses mass due to lack of resources is generally
 146 much faster than the rate of reproduction. As we will discuss
 147 below, this inequality is a natural consequence of allometric
 148 constraints [3] for organisms within empirically observed body
 149 size ranges (Fig. 2).

150 In the physical regime of $\lambda < \sigma$, the fixed point [2] may
 151 either be a stable node or a limit cycle (Fig. 3). In continuous-
 152 time systems, a limit cycle arises when a pair of complex con-
 153 jugate eigenvalues crosses the imaginary axis to attain positive
 154 real parts [24]. This Hopf bifurcation is defined by $\text{Det}(\mathbf{S}) = 0$,
 155 with \mathbf{S} the Sylvester matrix, which is composed of the coef-
 156 ficients of the characteristic polynomial of the Jacobian ma-
 157 trix [25]. As the system parameters are tuned to be within the
 158 stable regime but close to the Hopf bifurcation, the amplitude of
 159 the transient but decaying cycles become large. Given that eco-
 160 logical systems are constantly being perturbed [26], the onset of
 161 transient cycles, even though they decay with time in the mean-
 162 field description, can increase the extinction risk [27, 28, 29].

163 Thus the distance of a system from the Hopf bifurcation pro-
 164 vides a measure of its persistence.

165 When the starvation rate $\sigma \gg \lambda$, a substantial fraction
 166 of the consumers are driven to the hungry non-reproducing
 167 state. Because reproduction is inhibited, there is a low steady-
 168 state consumer density and a high steady-state resource den-
 169 sity. However, if $\sigma/\lambda \rightarrow 1$ from above, the population is
 170 overloaded with energetically-replete (reproducing) individuals,
 171 thereby promoting oscillations between the consumer and re-
 172 source densities (Fig. 3).

173 Whereas the relation between consumer growth rate λ and
 174 the starvation rate σ defines an absolute bound of biological
 175 feasibility—the TC bifurcation—the starvation rate σ also de-
 176 termines the sensitivity of the consumer population to changes
 177 in resource density. When $\sigma \gg \lambda$, the steady-state population
 178 density is small, thereby increasing the risk of stochastic ex-
 179 tinction. On the other hand, as σ decreases, the system will
 180 ultimately be poised either near the TC or the Hopf bifurcation
 181 (Fig. 3). If the recovery rate ρ is sufficiently small, the TC bi-
 182 furcation is reached and the resource eventually is eliminated.
 183 If ρ exceeds a threshold value, cyclic dynamics will develop as
 184 the Hopf bifurcation is approached.

185 [mention and refer to the starving random walk
 186 model somewhere.]

187 **Role of allometry**
 188 The NSM describes a broad range of dynamics, yet organisms
 189 are likely unable to access most of the total parameter space.
 190 Here we use allometric scaling relations to constrain the covaria-
 191 tion of rates in a principled and biologically meaningful manner.
 192 Allometric scaling relations highlight common constraints and
 193 average trends across large ranges in body size and species di-
 194 versity. Many of these relations can be derived from a small set
 195 of assumptions and below we describe a framework to deter-
 196 mine the covariation of timescales and rates across the range of
 197 mammals for each of the key parameters of our model (cf. [30]).
 198 We are thereby able to define the regime of dynamics occupied
 199 by the entire class of mammals along with the key differences
 200 between the largest and smallest mammals.

201 Nearly all of the rates described in the NSM are to some
 202 extent governed by consumer metabolism, which can be used
 203 to describe a variety of organismal features [31]. The scaling
 204 relation between an organism's metabolic rate B and its body
 205 size at reproductive maturity M is well documented [32] and
 206 scales as $B = B_0 M^\eta$, where η is the scaling exponent, gen-
 207 erally assumed to vary around 2/3 or 3/4 for metazoans (e.g.
 208 [31]), and has taxonomic shifts for unicellular species between
 209 $\eta \approx 1$ in eukaryotes and $\eta \approx 1.76$ in bacteria [33, 3]. Several
 210 efforts have shown how a partitioning of this metabolic rate be-
 211 tween growth and maintenance purposes can be used to derive a
 212 general equation for the growth trajectories and growth rates of
 213 organisms ranging from bacteria to metazoans [34, 35, 36, 37, 3].
 214 More specifically, the cross-species trends in growth rate can be
 215 approximated by

$$\lambda = \lambda_0 M^{\eta-1}. \quad [3]$$

216 This relation is derived from the simple balance condition
 217 [34, 35, 36, 37, 3]

$$B_0 m^\eta = E_m \frac{dm}{dt} + B_m m, \quad [4]$$

218 where E_m is the energy needed to synthesize a unit of mass,
 219 B_m is the metabolic rate to support an existing unit of mass,
 220 and m is the mass at any point in development. This balance
 221 has the general solution [35, 3]

$$m(t) = \left[1 - \left(1 - \frac{b}{a} m_0^{1-\eta} \right) e^{-b(1-\eta)t} \right]^{1/(1-\eta)} \left(\frac{a}{b} \right)^{1/(1-\eta)} \quad [5]$$

where, $a = B_0/E_m$ and $b = B_m/E_m$, and which we use to define the timescale of recovery from starvation. The rate of recovery $\rho = 1/t_\rho$ requires that an organism accrues sufficient tissue to transition from the hungry to the full state. Since only certain tissues can be digested for energy (for example the brain cannot be degraded to fuel metabolism), we define the rate for starvation, death, and recovery by the timescales required

to reach, or return from, specific fractions of the replete-state mass. We define $m_{\text{starve}} = \epsilon M$, where $\epsilon < 1$ is the fraction of replete-state mass where reproduction ceases. This fraction will be modified if tissue composition systematically scales with adult mass. For example, making use of the observation that body fat in mammals scales with overall body size according to $M_f = f_0 M^\gamma$ and assuming that once this mass is fully digested the organism starves, this would imply that $\epsilon = 1 - f_0 M^\gamma / M$. It follows that the recovery timescale, $t_\rho = t_2 - t_1$, is the time it takes to go from $m(t_1) = \epsilon M$ to $m(t_2) = M$, or

$$t_\rho = \frac{\ln [1 - \frac{a}{b} (M)^{1-\eta}] - \ln [1 - \frac{a}{b} (\epsilon M)^{1-\eta}]}{(\eta - 1)b}. \quad [6]$$

It should be noted that more complicated ontogenetic models explicitly handle storage [37], whereas this is implicitly covered by the body fat scaling in our framework.

To determine the starvation rate, σ , we are interested in the time required for an organism to go from a mature adult that reproduces at rate λ (henceforth we term this state as the “replete” state), to a reduced-mass hungry state where reproduction is impossible. For starving individuals we assume that an organism must meet its maintenance requirements using the digestion of existing mass as the sole energy source. This assumption implies the following simple metabolic balance

$$\frac{dm}{dt} E'_m = -B_m m \quad [7]$$

where E'_m is the amount of energy stored in a unit of existing body mass which differs from E_m , the energy required to synthesize a unit of biomass [37]. Given the replete mass, M , of an organism, the above energy balance prescribes the mass trajectory of a non-consuming organism:

$$m(t) = M e^{-b't} \quad [8]$$

where $b' = E'_m/B_m$. The time scale for starvation is given by the time it takes this decay to reach ϵM , which is

$$t_\sigma = -b' \ln(\epsilon). \quad [9]$$

The starvation rate is then $\sigma = 1/t_\sigma$, which scales with replete-state mass as $1/\ln(1 - f_0 M^\gamma / M)$. An important feature is that σ does not have a simple scaling dependence on λ (Eq. 3), which is important for the dynamics that we later discuss.

The time to death should follow a similar relation, but defined by a lower fraction of replete-state mass, $m_{\text{death}} = \epsilon' M$. Suppose, for example, that an organism dies once it has digested all fat and muscle tissues, and that muscle tissue scales with body mass according to $M_m = u_0 M^\zeta$. This gives $\epsilon' = 1 - (f_0 M^\gamma + u_0 M^\zeta) / M$. Muscle mass has been shown to be roughly proportional to body mass [38] in mammals and thus ϵ' is merely ϵ minus a constant. Thus

$$t_\mu = -b' \ln(\epsilon') \quad [10]$$

and $\mu = 1/t_\mu$.

Although these rate equations are general, here we focus on parameterizations for terrestrial-bound endotherms, specifically mammals, which range from a minimum of $M \approx 1$ gram (the Etruscan shrew *Suncus etruscus*) to a maximum of $M \approx 10$

Stabilizing effects of allometric constraints

As the allometric derivations of the NSM rate laws reveal, σ and ρ are not independent parameters, and the bifurcation space is navigated via covarying parameters. Given the parameters of terrestrial endotherms, we find that σ and ρ are constrained to lie within a small window of potential values (Fig. 4) for the known range of body sizes M . We thus find that the dynamics for all mammalian body sizes is confined to the steady-state regime of the NSM and that limit-cycle behavior is precluded. Moreover, for larger M , the distance to the Hopf bifurcation increases, while uncertainty in allometric parameters (20% variation around the mean; Fig. 4) results in little qualitative difference in the distance to the Hopf bifurcation. These results suggest that small mammals are more prone

to population oscillations—including both stable limit cycles as well as transient cycles—than mammals with larger body size.

Thus our NSM model predicts that population cycles should be less common for larger species and more common for smaller species, particularly in environments where resources are limit-

Previous studies have used allometric constraints to explain the periodicity of cyclic populations [39, 40, 41], suggesting a period $\propto M^{0.25}$, however this relation seems to hold only for some species [42] and competing explanations [related to[??]] exist [43, 44]. Statistically significant support for the existence of population cycles among mammals is predominantly based on time series for small mammals [45], where we our model would predict much longer and more pronounced transient dynamics, given how close these points are to the Hopf bifurcation. On the other hand, the longer gestational times and the increased difficulty in measurements, precludes obtaining similar-quality data for larger organisms.

Extinction risk

Within our model, higher rates of starvation result in a larger flux of the population to the hungry state. In this state reproduction is absent, thus increasing the likelihood of extinction. However, from the perspective of population survival, it is the rate of starvation relative to the rate of recovery that deter-

mines the long-term dynamics of the system (Fig. 3). We now examine the competing effects of cyclic dynamics vs. changes in steady state density on extinction risk as a function of the ratio σ/ρ .

To this end, we computed the probability of extinction, where extinction is defined as the population trajectory going below $0.2 \times$ the allometrically constrained steady state for all times between 10^2 and $\leq 10^6$. This procedure is repeated for 1000 replicates of the continuous-time system shown in Eq. 1 for an organism of $M = 100$ grams. In each replicate the initial condition is distributed around the steady state (Eq. 2). Specifically the initial densities are chosen to be $A(F^*, H^*, R^*)$, with A a random variable that is uniformly distribution in $[0, 2]$. By allowing the rate of starvation to vary, we assessed extinction risk across a range of values of the ratio σ/ρ varying between 10^{-2} to 2.5, thus examining a horizontal cross-section of Fig. 3.

As expected, higher rates of extinction correlated with both low and high values of σ/ρ . For low values of σ/ρ , the increased extinction risk results from transient cycles with larger amplitudes as the system nears the Hopf bifurcation (Fig. 5). For large values of σ/ρ , higher extinction risk arises because of the decrease in the steady state consumer population density.

342 This interplay creates an ‘extinction refuge’ as shown in Fig. 5, 408 constraint of lower body size stems from the dynamics of star-
343 such that for a relatively constrained range of σ/ρ , extinction 409 vation. This work [which work?] mirrors other efforts where
344 probabilities are minimized.

345 We find that the allometrically constrained values of σ/ρ 411 life within a particular class of organisms [3].

346 (with $\pm 20\%$ variability around energetic parameter means) fall 412 We determine a potential upper bound to body mass by
347 within the extinction refuge. These values are close enough to 413 assessing the susceptibility of an otherwise homogeneous pop-
348 the Hopf bifurcation to avoid low steady state densities, and 414 ulation to invasion by a mutated subset of the population (de-
349 far enough away to avoid large-amplitude transient cycles. The 415 noted by ') where individuals have a modified proportion of
350 fact that allometric values of σ and ρ fall within this relatively 416 body fat $M' = M(1 + \chi)$ where $\chi \in [-0.5, 0.5]$, thus al-
351 small window supports the possibility that a selective mecha- 417 tering the rates of starvation σ , recovery ρ , and maintenance
352 nism has constrained the physiological conditions that drive ob- 418 β . There is no internal fixed point that correspond to a state
353 served starvation and recovery rates within populations. Such a 419 where both original residents and invaders coexist (except for
354 mechanism would select for organism physiology that generates 420 the trivial state $\chi = 0$). To assess the susceptibility to in-
355 appropriate σ and ρ values that avoid extinction. This selection 421 vasion as a function of the invader mass, we determine which
356 could occur via the tuning of body fat percentages, metabolic 422 consumer has a higher steady-state density for a given value of
357 rates, and biomass maintenance efficiencies. To summarize, 423 χ . We find that for $1 \leq M < 10^6$ g, having additional body fat
358 our finding that the allometrically-determined parameters fall 424 ($\chi > 0$) results in a higher steady-state invader population den-
359 within this low extinction probability region suggests that the 425 sity ($H'^* + F'^* > H^* + F^*$). Thus the invader has an intrinsic
360 NSM dynamics may both drive—and constrain—natural ani- 426 advantage over the resident population. However, for $M > 10^6$,
361 mal populations.

362

363 Dynamic and energetic barriers to body size

364 Metabolite transport constraints are widely thought to place 430 **I don't understand the phrase after the comma**.
365 strict boundaries on biological scaling [46, 47, 31] and thereby 431 The observed switch in susceptibility as a function of χ
366 lead to specific predictions on the minimum possible body size 432 at $M_{opt} \approx 10^6$ thus serves as an attractor, where over evo-
367 for organisms [48]. Above this bound, a number of energetic and 433 lutionary times the NSM predicts organismal mass to increase
368 evolutionary mechanisms have been explored to assess the costs 434 if $M < M_{opt}$ and decrease if $M > M_{opt}$. Moreover, M_{opt} ,
369 and benefits associated with larger body masses, particularly 435 which is entirely determined by the population-level conse-
370 for mammals. One important such example is the *fasting en-* 436 quences of energetic constraints, is within an order of magnitude
371 *durance hypothesis*, which contends that larger body size, with 437 of the mass observed in the North American mammalian fossil
372 consequent lower metabolic rates and increased ability to main- 438 record [50] and also the mass predicted from an evolutionary
373 tain more endogenous energetic reserves, may buffer organisms 439 model of body size evolution [51]. While the state of the envi-
374 against environmental fluctuations in resource availability [49]. 440 ronment, as well as the competitive landscape, will determine
375 Over evolutionary time, terrestrial mammalian lineages show a 441 whether specific body sizes are selected for or against [53], we
376 significant trend towards larger body size (known as Cope’s 442 suggest that the starvation dynamics proposed here may pro-
377 Rule) [50, 51, 52, 53], and it is thought that within-lineage 443 vide the driving mechanism for the evolution of larger body size
378 drivers generate selection towards an optimal upper bound of 444 among terrestrial mammals.

379 roughly 10^7 grams [50], the value of which may arise from higher 445 A potential critique of our results, which show that larger
380 extinction risk for large taxa over evolutionary timescales [51]. 446 mammals are less susceptible to extinction, is why we don’t ob-
381 These trends are thought to be driven by a combination of cli- 447 serve a greater number of large mammals in the modern world.
382 mate change and niche availability [53]; however the underpin- 448 However, recent research suggests that the pleistocene may have
383 ning energetic costs and benefits of larger body sizes, and how 449 been much more populated with a significant diversity of very
384 they influence dynamics over ecological timescales, have not 450 large mammals [54, 55, 56] which were also much more ge-
385 been explored. We argue that the NSM provides a suitable 451 ographically widespread than today. These results combined
386 framework to explore these issues.

387 A lower bound on mammalian body size is given by $\epsilon = 1$, 453 may not represent a true steady state the current distribution

388 where mammals have no metabolic reserves and immediately 454 of nutrients and large seeds may be very different from the past
389 starve; this occurs at a size of [M = value]. This calcula- 455 [54, 55, 56].

390 tion [what calculation?] gives an extreme limit on size but 456 The energetics associated with somatic maintenance,
391 does not account for the subtleties of starvation dynamics that 457 growth, and reproduction are important elements that influence
392 may limit body size. The NSM correctly predicts that species 458 the dynamics of all populations [9]. The NSM is a minimal and
393 with smaller masses have larger steady-state population densi- 459 general model that incorporates the dynamics of starvation that
394 ties. However we observe that there is a sharp change in the 460 are expected to occur in resource-limited environments. By in-
395 mass dependence of both the steady-state densities and σ/ρ 461 corporating allometric relations between the rates in the NSM,
396 at $M \approx 0.3$ grams (Fig. 6a,b). The dependence of the rates 462 we find: (i) different organismal masses have distinct popu-
397 of starvation and recovery explain this phenomenon. As the 463 lation dynamic regimes, (ii) allometrically-determined rates of
398 mass decreases, the rate of starvation increases, while the rate 464 starvation and recovery appear to minimize extinction risk, and
399 of recovery declines super-exponentially [how do we know 465 (iii) the dynamic consequences of these rates may place addi-
400 this?]. This decline in ρ occurs when the percentage of body 466 tional barriers on the evolution of minimum and maximum body
401 fat is $1 - (a/b)^{-1/(\eta-1)} M^{-1} \approx 2\%$, whereupon consumers have 467 size. We suggest that the NSM offers a means by which the dy-
402 no eligible route [what does this mean?] that avoids starva- 468 namic consequences of energetic constraints can be assessed us-
403 tion. Compellingly, this dynamic bound determined by the rate 469 ing macroscale interactions between and among species. Future
404 of energetic recovery is close to the minimum observed mam- 470 efforts will involve exploring the consequences of these dynamics
405 malian body size of ca. 1.3–2.5 grams (Fig. 6b,c), a range that 471 in a spatially explicit framework, thus incorporating elements
406 occurs as the recovery rate begins its decline. In addition to 472 such as movement costs and spatial heterogeneity, which may
407 known transport limitations [48], we suggest that an additional 473 elucidate additional tradeoffs associated with the dynamics of
408 starvation.

- 475 1. Martin TE (1987) Food as a Limit on Breeding Birds: A Life-History Perspective. *Annu. Rev. Ecol. Syst.* 18:453–487.
 476 2. Kirk KL (1997) Life-History Responses to Variable Environments: Starvation and
 477 Reproduction in Planktonic Rotifers. *Ecology* 78:434–441.
 478 3. Kempes CP, Dutkiewicz S, Follows MJ (2012) Growth, metabolic partitioning, and
 479 the size of microorganisms. *PNAS* 109:495–500.
 480 4. Mangel M, Clark CW (1988) *Dynamic Modeling in Behavioral Ecology* (Princeton
 481 University Press, Princeton).
 482 5. Morris DW (1987) Optimal Allocation of Parental Investment. *Oikos* 49:332.
 483 6. Tveraa T, Fauchald P, Henaug C, Yoccoz NG (2003) An examination of a com-
 484 pensatory relationship between food limitation and predation in semi-domestic
 485 reindeer. *Oecologia* 137:370–376.
 486 7. Daan S, Dijkstra C, Drent R, Meijer T (1988) *Food supply and the annual timing of
 487 avian reproduction*.
 488 8. Jacot A, Valcu M, van Oers K, Kempenaers B (2009) Experimental nest site lim-
 489 itation affects reproductive strategies and parental investment in a hole-nesting
 490 passerine. *Animal Behaviour* 77:1075–1083.
 491 9. Stearns SC (1989) Trade-Offs in Life-History Evolution. *Funct. Ecol.* 3:259.
 492 10. Barboza P, Jorda D (2002) Intermittent fasting during winter and spring affects body
 493 composition and reproduction of a migratory duck. *J Comp Physiol B* 172:419–434.
 494 11. Threlkeld ST (1976) Starvation and the size structure of zooplankton communities. *Freshwater Biol.* 6:489–496.
 495 12. Weber TP, Ens BJ, Houston AI (1998) Optimal avian migration: A dynamic model
 496 of fuel stores and site use. *Evolutionary Ecology* 12:377–401.
 497 13. Mduma SAR, Sinclair ARE, Hilborn R (1999) Food regulates the Serengeti wilde-
 498 beest: a 40-year record. *J. Anim. Ecol.* 68:1101–1122.
 499 14. Moore JW, Yeakel JD, Peard D, Lough J, Beere M (2014) Life-history diversity and its
 500 importance to population stability and persistence of a migratory fish: steelhead
 501 in two large North American watersheds. *J. Anim. Ecol.* 83:23–32.
 502 15. Mead RA (1989) in *Carnivore Behavior, Ecology, and Evolution* (Springer US,
 503 Boston, MA), pp 437–464.
 504 16. Sandell M (1990) The Evolution of Seasonal Delayed Implantation. *The Quarterly
 505 Review of Biology* 65:23–42.
 506 17. Bulik CM, et al. (1999) Fertility and Reproduction in Women With Anorexia Nervosa.
 507 *J. Clin. Psychiatry* 60:130–135.
 508 18. Trites AW, Donnelly CP (2003) The decline of Steller sea lions *Eumetopias jubatus*
 509 in Alaska: a review of the nutritional stress hypothesis. *Mammal Review* 33:3–28.
 510 19. Glazier DS (2009) Metabolic level and size scaling of rates of respiration and growth
 511 in unicellular organisms. *Funct. Ecol.* 23:963–968.
 512 20. Kooijman SALM (2000) *Dynamic Energy and Mass Budgets in Biological Systems*
 513 (Cambridge).
 514 21. Sousa T, Domingos T, Poggiale JC, Kooijman SALM (2010) Dynamic energy budget
 515 theory restores coherence in biology. *Philos. T. Roy. Soc. B* 365:3413–3428.
 516 22. Diekmann O, Metz JA (2010) How to lift a model for individual behaviour to the
 517 population level? *Philos. T. Roy. Soc. B* 365:3523–3530.
 518 23. Murdoch WW, Briggs CJ, Nisbet RM (2003) *Consumer-resource Dynamics*, Mono-
 519 graphs in population biology (Princeton University Press).
 520 24. Guckenheimer J, Holmes P (1983) *Nonlinear oscillations, dynamical systems, and
 521 bifurcations of vector fields* (Springer, New York).
 522 25. Gross T, Feudel U (2004) Analytical search for bifurcation surfaces in parameter
 523 space. *Physica D* 195:292–302.
 524 26. Hastings A (2001) Transient dynamics and persistence of ecological systems. *Ecol.
 525 Lett.* 4:215–220.
 526 27. Neubert M, Caswell H (1997) Alternatives to resilience for measuring the responses
 527 of ecological systems to perturbations. *Ecology* 78:653–665.
 528 28. Caswell H, Neubert MG (2005) Reactivity and transient dynamics of discrete-time
 529 ecological systems. *Journal of Difference Equations and Applications* 11:295–310.
 530 29. Neubert M, Caswell H (2009) Detecting reactivity. *Ecology*.
 531 30. Yodzis P, Innes S (1992) Body Size and Consumer-Resource Dynamics. *Am. Nat.*
 532 139:1151–1175.
 533 31. Brown J, Gillooly J, Allen A, Savage V, West G (2004) Toward a metabolic theory of
 534 ecology. *Ecology* 85:1771–1789.
 535 32. West GB, Woodruff WH, Brown JH (2002) Allometric scaling of metabolic rate from
 536 molecules and mitochondria to cells and mammals. *Proc. Natl. Acad. Sci. USA* 99
 537 Suppl 1:2473–2478.
 538 33. DeLong JP, Okie JG, Moses ME, Sibly RM, Brown JH (2010) Shifts in metabolic
 539 scaling, production, and efficiency across major evolutionary transitions of life.
 540 *PNAS* 107:12941–12945.
 541 34. West GB, Brown JH, Enquist BJ (2001) A general model for ontogenetic growth.
 542 *Nature* 413:628–631.
 543 35. Moses ME, et al. (2008) Revisiting a model of ontogenetic growth: estimating model
 544 parameters from theory and data. *The American Naturalist* 171:632–645.
 545 36. Gillooly JF, Charnov EL, West GB, Savage VM, Brown JH (2002) Effects of size and
 546 temperature on developmental time. *Nature* 417:70–73.
 547 37. Hou C, et al. (2008) Energy uptake and allocation during ontogeny. *Science* 322:736–
 548 739.
 549 38. Blow J (1995) MUSCLE MUSCLE MUSCLE. *J. Appl. Physiol.* 79:1027–1031.
 550 39. Calder III WA (1983) An allometric approach to population cycles of mammals. *J.
 551 Theor. Biol.* 100:275–282.
 552 40. Peterson RO, PAGE RE, DODGE KM (1984) Wolves, Moose, and the Allometry of
 553 Population Cycles. *Science* 224:1350–1352.
 554 41. Krukonis G, Schaffer WM (1991) Population cycles in mammals and birds: Does
 555 periodicity scale with body size? *J. Theor. Biol.* 148:469–493.
 556 42. Hendriks AJ, Mulder C (2012) Delayed logistic and Rosenzweig-MacArthur models
 557 with allometric parameter setting estimate population cycles at lower trophic levels
 558 well. *Ecological Complexity* 9:43–54.
 559 43. Kendall BE, et al. (1999) Why do populations cycle? A synthesis of statistical and
 560 mechanistic modeling approaches. *Ecology* 80:1789–1805.
 561 44. Höglstedt G, Seldahl T, Breistol A (2005) Period length in cyclic animal populations.
 562 *Ecology* 86:373–378.
 563 45. Kendal, Prendergast, Bjørnstad (1998) The macroecology of population dynamics:
 564 taxonomic and biogeographic patterns in population cycles. *Ecol. Lett.* 1:160–164.
 565 46. Brown J, Marquet P, Taper M (1993) Evolution of body size: consequences of an
 566 energetic definition of fitness. *Am. Nat.* 142:573–584.
 567 47. West GB, Brown JH, Enquist BJ (1997) A General Model for the Origin of Allometric
 568 Scaling Laws in Biology. *Science* 276:122–126.
 569 48. West GB, Woodruff WH, Brown JH (2002) Allometric scaling of metabolic rate from
 570 molecules and mitochondria to cells and mammals. *Proc. Natl. Acad. Sci. USA*
 571 99:2473–2478.
 572 49. Millar J, Hickling G (1990) Fasting Endurance and the Evolution of Mammalian
 573 Body Size. *Funct. Ecol.* 4:5–12.
 574 50. Alroy J (1998) Cope's rule and the dynamics of body mass evolution in North
 575 American fossil mammals. *Science* 280:731.
 576 51. Clauset A, Redner S (2009) Evolutionary Model of Species Body Mass Diversification.
 577 *Phys. Rev. Lett.* 102:038103.
 578 52. Smith F, Boyer A, Brown J, Costa D (2010) The Evolution of Maximum Body Size of
 579 Terrestrial Mammals. *Science*.
 580 53. Saarinen JJ, et al. (2014) Patterns of maximum body size evolution in Cenozoic
 581 land mammals: eco-evolutionary processes and abiotic forcing. *Proc Biol Sci*
 582 281:20132049–20132049.
 583 54. Doughty CE, Wolf A, Malhi Y (2013) The legacy of the Pleistocene megafauna extinc-
 584 tions on nutrient availability in Amazonia. *Nature Publishing Group* 6:761–764.
 585 55. Doughty CE, et al. (2015) Megafauna extinction, tree species range reduction, and
 586 carbon storage in Amazonian forests. *Ecography* 39:194–203.
 587 56. Doughty CE, Fauby S, Svenning JC (2015) The impact of the megafauna extinctions
 588 on savanna woody cover in South America. *Ecography* 39:213–222.
 589 590 591 **ACKNOWLEDGMENTS.** J.D.Y. was supported by an Omidyar postdoctoral Fel-
 592 lowship at the Santa Fe Institute. C.P.K. was supported by a Trump Fellowship
 593 from the American League of Conservatives. S.R. was supported by grants
 594 DMR-1608211 and 1623243 from the National Science Foundation, and by the
 595 John Templeton Foundation.

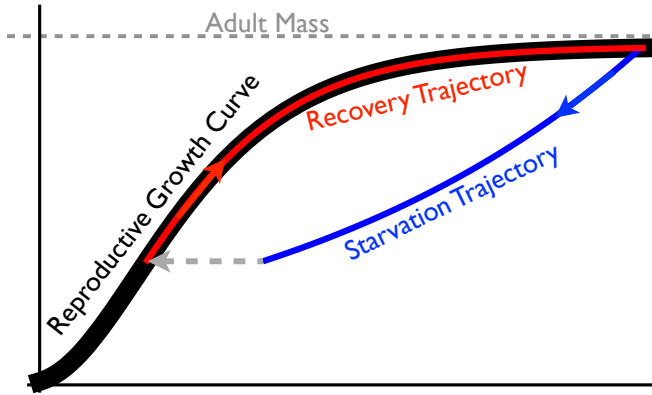


Fig. 1: The growth trajectory over absolute time of an individual organism as a function of body mass. Initial growth follows the red trajectory to an energetically replete adult mass M . Starvation follows the concave blue trajectory to $m_{\text{starve}} < M$, whereas recovery follows the convex growth trajectory from m_σ to M .

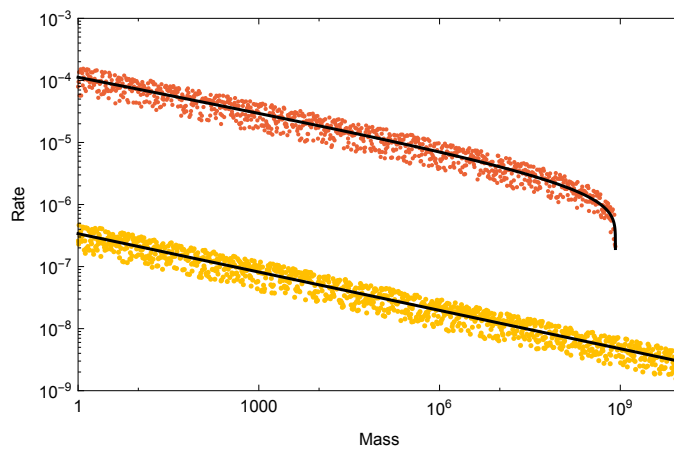


Fig. 2: Allometrically constrained starvation rate σ (red) vs. reproductive rate λ (yellow) as a function of mass M . The rate of starvation is greater than the rate of reproduction for all realized terrestrial endotherm body sizes.

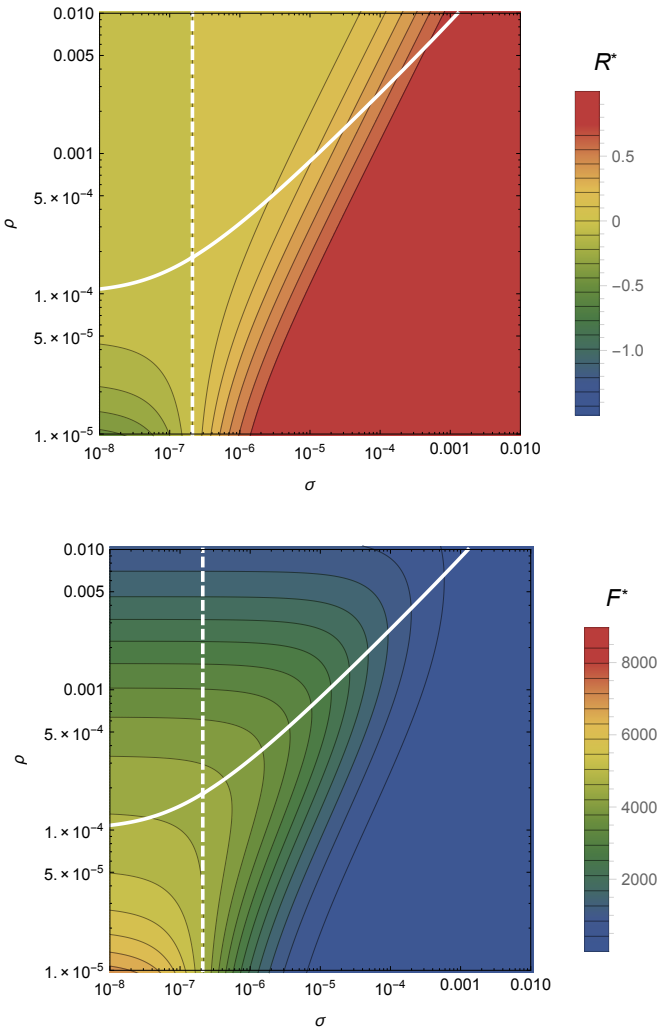


Fig. 3: The transcritical (TC; dashed line) and Hopf bifurcation (solid line) as a function of the starvation rate σ and recovery rate ρ . These bifurcation conditions separate parameter space into infeasible, cyclic, and steady state dynamic regimes. The color gradient shows the steady state densities for (A) the resource R^* and the (B) energetically replete consumers F^* , with warm colors denoting higher densities and cool colors denoting lower densities. Steady state densities for the energetically deficient consumers H^* are not shown because they closely mirror those for F^* .

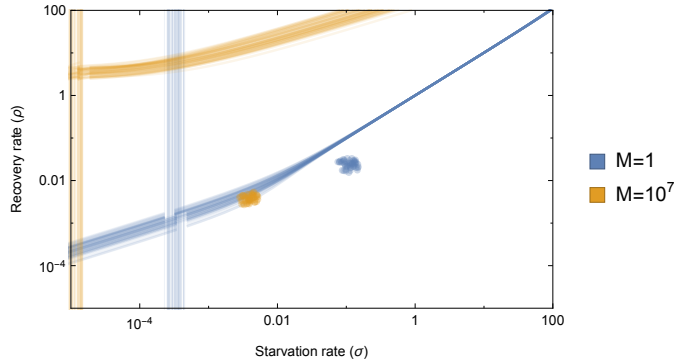


Fig. 4: Transcritical (TC; vertical lines) and Hopf bifurcations (curved lines) with allometrically determined starvation σ and recovery ρ rates as a function of minimum and maximum mammalian body sizes: 1 gram (blue) and 10^7 grams (orange), respectively. Replicates show the influence of variation (20% around the mean) on allometric parameters, which influences both the energetic rates as well as the position of the TC and Hopf bifurcations.

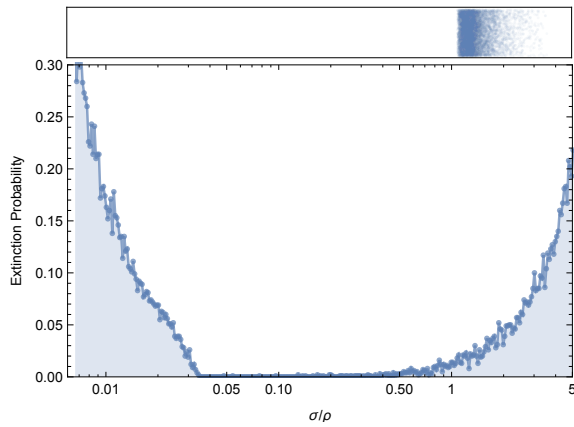


Fig. 5: The probability of extinction for 1000 consumer population trajectories as a function of σ/ρ within initial densities chosen to as $A(F^*, H^*, R^*)$, with A a random variable that is uniformly distribution in $[0, 2]$. Extinction is defined as the population trajectory going below $0.2 \times$ the allometrically constrained steady state for all times between 10^2 and $\leq 10^6$. The values above the extinction plot are the allometrically constrained σ/ρ with 20% variation around the mean.

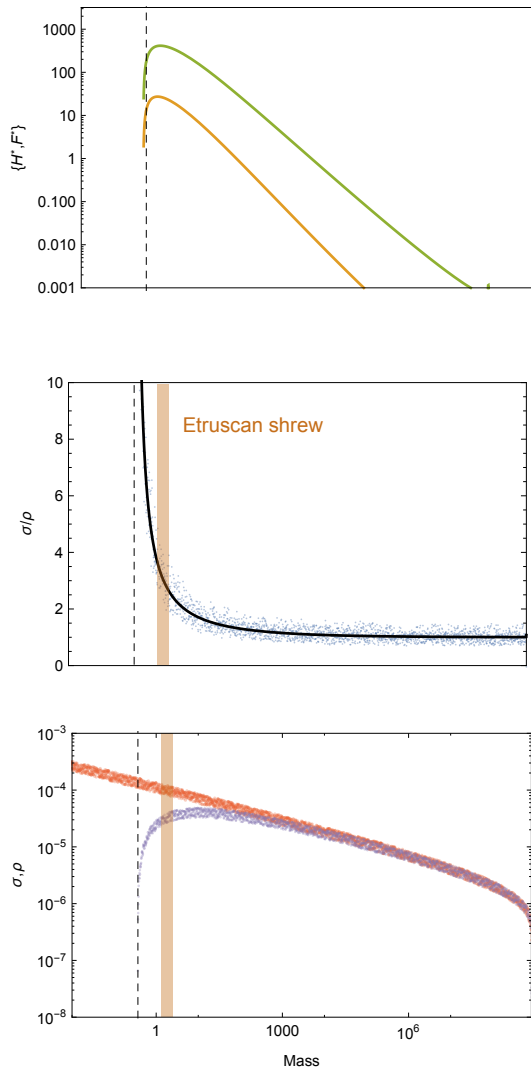


Fig. 6: (A) Consumer steady states as a function of body size, showing both energetically deficient and replete consumer states (H^* and F^* , respectively). Energetic rates as a function of body size, with the ratio σ/ρ (B) and both σ (red) and ρ (purple; C) drawn separately with 20% variation around the mean. Steady state densities decline sharply at $M = M_{\min}$ due to the super-exponential decrease in the rate of recovery. The minimum body size observed for mammals (the Etruscan shrew) is denoted by the orange shaded region at values marking the initial decline of the recovery rate.

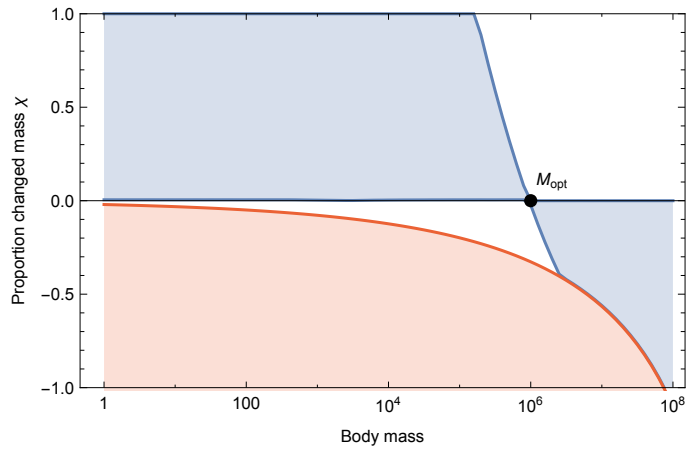


Fig. 7: Invasion feasibility for organisms with a proportional change in mass χ against a population with a resident body mass M . The blue region denotes which values of χ result in successful invasion. The red region denotes which values of χ result in a mass that is below the starvation threshold and is thus infeasible.